PHYSICAL REVIEW B VOLUME 52, NUMBER 24 15 DECEMBER 1995-II

ARTICLES

Fundamental studies on the structures and properties of some B_{12}-based crystals

Dong Li and W. Y. Ching
Department of Physics, University of Missouri-Kansas City, Kansas City, Missouri 64110
(Received 22 May 1995; revised manuscript received 3 August 1995)

The first-principles orthogonalized linear combination of atomic orbitals method has been applied to calculate the electronic structures, total energies, and optical properties of four boron-rich compounds: $B_{12}As_2$, $B_{12}P_2$, $B_{11}C(CBC)$ (or B_4C), and $B_{13}C_2$. The band structures show that $B_{12}As_2$, $B_{12}P_2$, $B_{11}C(CBC)$ are semiconductors with indirect band gaps while $B_{13}C_2$ is a metal with an intrinsic hole at the top of the valence band below a semiconductorlike gap. The calculated density of states are resolved into atomic and orbital partial components and the valence-charge distributions are also studied. The natural bonding characteristics in these crystals are illuminated by evaluating the Mulliken effective charges on each atom and overlap populations between pairs of atoms. It is shown that intericosahedral bonding is much stronger than the intraicosahedral bonding. The chain elements in $B_{12}As_2$ and $B_{12}P_2$ donate electrons to the icosahedra while in the other two crystals, they gain a slight amount of charge in forming strong covalent bonds. The bulk moduli of these crystals are estimated by means of total-energy calculation as a function of crystal volume, and are to be considered as upper limits. We have also calculated the interband optical conductivities and the complex dielectric functions in these crystals. Static dielectric constants for the three semiconductors are estimated to be 6.59, 5.49, and 6.35, respectively, which are in good agreement with recent experimental measurements. The bulk plasmon excitations in these four crystals are found to be in the 30–34-eV range.

I. INTRODUCTION

Boron and boron-rich compounds form an interesting class of materials with many diversified and fascinating properties.[1–5] They exist in different phases in a variety of crystal structures including cubic, rhombohedral, and tetragonal phases.[6] These stable refractory materials have conductivities that stretch from that of a metal to that of a wide-band-gap insulator. The basic structural units in these B compounds are various polyhedra such as icosahedron, octahedron, or cubooctahedron,[7] with the icosahedron B_{12} with 12 B atoms the most common one. It is significant that icosahedral framework in B or B-rich solids such as the complex β-rhombohedral boron (β-rB_{105}) is stable over a wide range of pressure, indicating a strong intericosahedron bonding.[1] It has long been recognized that the B atom, with its three valence electrons, is insufficient to form bonds for the four low-lying orbitals. Theoretical analysis shows that the B_{12} icosahedron is two-electron deficient in a setting for the 13 internal bonding orbitals and 12 external equivalent orbitals.[8] The general viewpoint on the means of supplying the two missing electrons is to either replace the B atom within the icosahedron with another atom of higher valency, or to connect the equatorial B atoms of the three adjacent B_{12} icosahedra with an interstitial chain of atoms involving group-IV or -V elements which can supply the electrons for the required bonding.[9] In the simplest case of the α phase of rhombohedron boron (α-rB_{12}), however, a weak three-center bond can be formed by the equatorial B atoms between the icosahedra which contribute two electrons.[2] If we consider B_{12} to be a molecular unit, it is interesting to note that in the B-rich compounds, in contrast to other molecular solids, the intermolecular bonding between icosahedra appears to be stronger than intramolecular bonding. This type of crystal has been called an inverted molecular solid.[2,10] This is quite different from fullerene (C_{60})-based compounds where the forces between the bucky balls are of the weak van der Waal type. It is also interesting to point out that both α-rB_{12} and C_{60} in the fcc lattice are semiconductors with comparable sizes of band gap.[11,12]

There have been many recent experimental[13–20] and theoretical[21–28] investigations of the structures and properties of B and B-rich compounds. In particular, the structure of the B_4C phase has been the subject of much controversy. Determination of x in $B_{1-x}C_x$ compounds and the precise location of the C atoms has attracted intense research efforts.[3,4] It has been concluded that two of the compounds $B_{12}(CBC)$ ($x=0.13$) and $B_{11}C(CBC)$ ($x=0.2$) with a C-B-C intericosahedral chain are more stable. Other B_{12}-based compounds have also attracted considerable interest because of their unique combination of structures and properties.[20,27,28]

In this paper, we report a systematic study of the fundamental properties of four B_{12}-based compounds. These are $B_{12}As_2$, $B_{12}P_2$, $B_{11}C(CBC)$, and $B_{13}C_2$. A similar study on pure B_{12}-based crystals has been reported be-

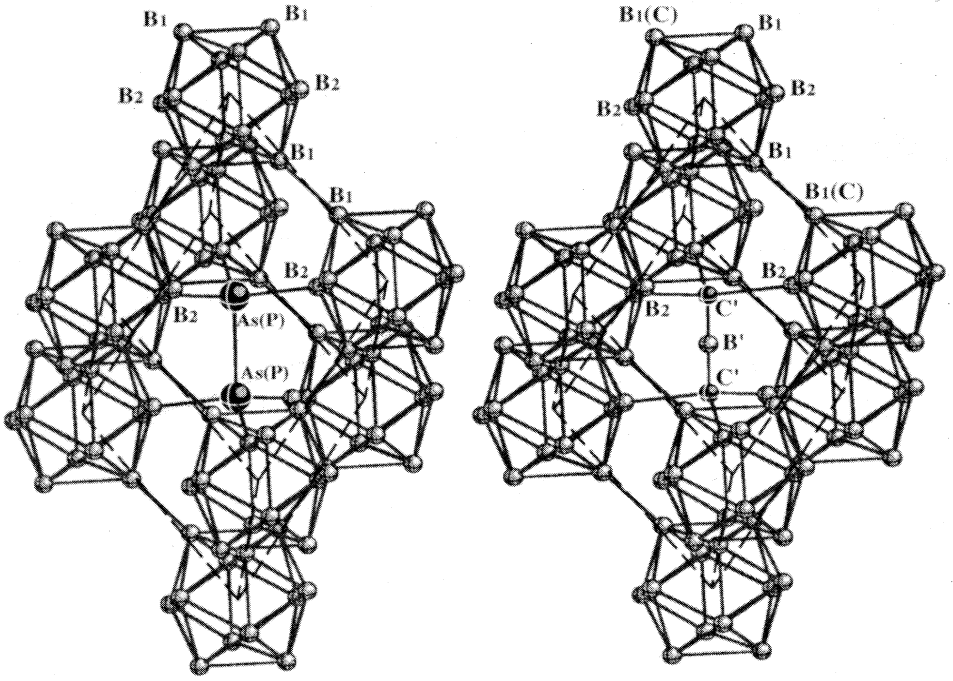

FIG. 1. Sketch of the crystal structure. (a) $B_{12}As_2$ or $B_{12}P_2$. (b) $B_{13}C_2$ or $B_{11}C(CBC)$. The dashed frame represents the rhombohedral unit cell.

fore.[12] We briefly describe the crystal structures in Sec. II, and method of calculations in Sec. III. Results on the electronic structure and crystal bonding are presented in Secs. IV and V, respectively, while those of total energies and optical properties are discussed in Secs. VI and VII. Section VIII summarizes some conclusions.

II. CRYSTAL STRUCTURES

Morosin *et al.*[29] measured the crystal structures of $B_{12}As_2$, $B_{12}P_2$, and $B_{13}C_2$ and atomic positions using single-crystal x-ray diffraction. Bylander, Kleinman, and Lee predicted the crystal parameters of $B_{11}C(CBC)$ based

TABLE I. Crystal data and calculated electronic structures for B_{12}-based crystals.

	$B_{12}As_2$	$B_{12}P_2$	$B_{13}C_2$	$B_{11}C(CBC)$
Lattice constant (Å)	$a=5.3333$	$a=5.2559$	$a=5.1850$	$a=5.1425$
	$\alpha=70.505°$	$\alpha=69.620°$	$\alpha=65.590°$	$\alpha=65.758°$
Density (g/cm^3)	3.56	2.58	2.47	2.55
Cell volume (Å^3)	130.52	123.25	110.54	108.15
Space group	$R\bar{3}m$	$R\bar{3}m$	$R\bar{3}m$	$R\bar{3}m$
Band gap (eV)	2.78($Z\rightarrow A$)	2.63($Z\rightarrow A$)	3.01($A\rightarrow A$)	3.04($Z\rightarrow A$)
Direct gaps:	4.81(Γ)	4.75(Γ)	3.48(Γ)	5.54(Γ)
	4.21(X)	4.06(X)	4.14(X)	3.70(X)
	3.07(Z)	3.10(Z)	3.48(Z)	3.55(Z)
	2.97(A)	2.83(A)	3.01(A)	3.56(A)
	4.21(D)	4.06(D)	3.01(D)	3.70(D)
Expt. gap (eV)	3.47[a]	3.35[a]		
other calculation	2.609[b]($\Gamma\rightarrow A$)		2.915[c]($B\rightarrow A$)	2.781[d]($B\rightarrow A$)
Bandwidths (eV)				
upper VB	7.69	8.05	8.85	8.95
total VB	15.08	15.03	15.79	16.06

[a]Reference 13.
[b]Reference 26.
[c]Reference 24.
[d]Reference 24.

on the *ab initio* pseudopotential calculation.[24] All four crystals $B_{12}As_2$, $B_{12}P_2$, $B_{11}C(CBC)$, and $B_{13}C_2$ have the same space group $R\bar{3}m$ as the α-r-B_{12}. The structure of these phases consists of a rhombohedral packing of B or B-rich icosahedra bonded to one another through a two or three-atom chain along the z axis. This is illustrated in Fig. 1. Figure 1(a) shows a two-atom chain (As-As or P-P) connecting to six icosahedra in $B_{12}As_2$ or $B_{12}P_2$. Figure 1(b) shows a three-atom chain (C'-B'-C') substituting for the two-atom chain and links in the same fashion for $B_{11}C(CBC)$ or $B_{13}C_2$ crystals. The dashed frame in Fig. 1(a) or 1(b) depicts the rhombohedral unit cell for the crystal. The introduction of a two- or three-atom chain to α-r-B_{12} induces substantial deformation of the icosahedron. Because of the different local bonding environment, we labeled as B_1 the top or bottom B atoms, and as B_2 the equatorial B atoms in the icosahedron, and use B' and C' to represent the chain atoms. In $B_{11}C(CBC)$, one C atom occupies the vertex position of the icosahedron and externally bonds to a B atom from another icosahedron. The symmetry of the B_{12} icosahedron is distorted because of the C substitution. Along the interstitial chains, As-As has the largest bond length of 2.39 Å, which is about 0.15 Å longer than the P-P bond. The bond lengths between C' and B' for the three-atom chain in $B_{13}C_2$ and $B_{11}C(CBC)$ crystals are between 1.43 and 1.45 Å. The intraicosahedral bond lengths vary from 1.74 to 1.81 Å, while the intericosahedral bond length is around 1.73 Å. Among the four crystals, $B_{12}As_2$ has the largest lattice constant, rhombohedral angle α, and density due to the interstitial chain of the large-size As atoms. The structural data of the four crystals are summarized in Table I.

III. METHOD OF COMPUTATION

We have used the self-consistent orthogonalized linear combination of atomic orbital (OLCAO) method, with the local-density approximation (LDA) of the density-functional theory to calculate the band structures and ground-state properties of the four B_{12}-based crystals. The resulting wave functions were used to study optical transitions in these crystals. Since the computational method has been well described elsewhere,[30] only a brief account is given here. The basis functions are atomic functions expressed as linear combinations of Gaussian-type orbitals. A full basis set was used in all calculations. The crystal potential and charge density were also expressed as sums of atom-centered functions consisting of s-type Gaussians. The Wigner interpolation formula was used to account for the additional correlation effect.[31] Our judicious choice of fitting functions resulted in fitting errors of no more than 0.001 electron per valence electron in all four crystals. In the self-consistent iterative procedure, six special-**k** points were used for Brillouin-zone (BZ) integration. For the density of states (DOS) and optical calculations, 110 regularly spaced **k** points in the irreducible part of the BZ were used for solving the energy eigenvalues and eigenfunctions. The DOS's were calculated using the linear analytical tetrahedron method and the partial DOS's (PDOS's) were evaluated using the Mulliken procedure.[32]

In an atomic wave-based method for electronic structure studies, it is instructive to study the charge transfer and the strength of covalent bonding by evaluating the effective charge on each atom and the overlap population or bond orders between a pair of atoms. Positive or negative population values for a specific pair of atoms provide a simple way to characterize the bonding, net bonding, or antibonding. Tanaka and Niihara used this approach to study the bonding of solute atoms in β-Si_3N_4 using the DV-$X\alpha$ method.[33] In the OLCAO method, the single-particle wave function $\psi_n(r)$ and overlap matrix $S_{i\gamma,j\delta}$ are given by

$$\psi_n(\mathbf{r})=\sum_{i,\gamma} A_{i,\gamma}(\mathbf{k})b_{i,\gamma}(\mathbf{k},\mathbf{r}) , \tag{1}$$

$$S_{i\gamma,j\delta}(\mathbf{k})=\langle b_{i,\gamma}(\mathbf{k},\mathbf{r})|b_{j,\delta}(\mathbf{k},\mathbf{r})\rangle , \tag{2}$$

where $b_{i\gamma}(\mathbf{k},\mathbf{r})$ is the Bloch function constructed from atomic or atomiclike orbitals, and $S_{i\gamma j\delta}(\mathbf{k})$ is the overlap integral at **k**. $A_{i\gamma}$ are eigenfunction coefficients, γ,δ and i,j represent atomic and orbital specifications, respectively. The effective charge Q_δ^* on atom δ and the overlap population $\rho_{\gamma,\delta}$ between atoms γ and δ can be expressed as

$$Q_\delta^*=\sum_{n=\text{occ.}}\sum_{i}\sum_{j,\gamma}\sum_{\mathbf{k}} W(\mathbf{k})(A_{i,\gamma}^n)^* A_{j,\delta}^n S_{i\gamma,j\delta}(\mathbf{k}) , \tag{3}$$

$$\rho_{\gamma,\delta}=\sum_{n=\text{occ.}}\sum_{i}\sum_{j}\sum_{\mathbf{k}} W(A_{i,\gamma}^n)^* A_{j,\delta}^n S_{i\gamma,j\delta}(\mathbf{k}) . \tag{4}$$

The summation is over the entire BZ, and $W(\mathbf{k})$ is the **k**-point weighting factor. Because the Mulliken scheme is less valid when the basis functions are extended, such as when a full basis set is used, we used a minimal basis set in evaluating Q_δ^* and $\rho_{\gamma,\delta}$.

The total energies of the crystals are evaluated as a function of cell volume in accordance with the LDA theory:

$$E_T=\sum_{n,k}^{\text{occ}} E_n(\mathbf{k})+\int \rho(\mathbf{r})(\varepsilon_{\text{XC}}-V_{\text{XC}}-V_{e\text{-}e}/2)d\mathbf{r} + \sum_{\gamma,\delta} Z_\gamma Z_\delta/(\mathbf{R}_\gamma-\mathbf{R}_\delta) , \tag{5}$$

where $E_n(\mathbf{k})$ is the band energy, $\rho(\mathbf{r})$ represents the crystal charge density. V_{XC} and $V_{e\text{-}e}$ are the exchange-correlation potential and electron-electron Coulomb potential, respectively, while ε_{XC} is exchange-correlation energy functional.

In the present total-energy calculation, the lattice constants of the crystals are scaled to obtain an expanded or contracted crystal volume, while assuming the crystal symmetries are not reduced. In principle, other crystal parameters such as the c/a ratio and internal coordinates should be optimized by searching for the minimum in the total energy in the multidimensional parameter space. Such a procedure is still computationally prohibitive for us at this time. The bulk modulus or the compressibility

are then obtained by fitting the calculated total-energy data points to Murnaghan's equation of state.[34] Because of the fact that the internal parameters were not optimized, our calculated bulk modulus near the equilibrium volume should be considered as upper limits only.

From the energy eigenvalues and wave functions, the real part of the frequency-dependent interband optical conductivity $\sigma(\omega)$ can be obtained according to

$$\sigma(\hbar\omega)=\frac{e^2}{(2\pi)^2\mu\hbar\omega}\int d\mathbf{k}\sum_{n,m}|\langle\psi_m(\mathbf{k},\mathbf{r})|\mathbf{p}|\psi_n(\mathbf{k},\mathbf{r})\rangle|^2 f_n(\mathbf{k})[1-f_m(\mathbf{k})]\delta[E_m(\mathbf{k})-E_n(\mathbf{k})-\hbar\omega]\ , \tag{6}$$

where $\hbar\omega$ is the photon energy, and f_n is the Fermi function for state n. The anisotropy of the conductivity can be investigated from the components of the square of the momentum matrix element, $|\langle\psi_m|\mathbf{p}|\psi_n\rangle|^2$ in Cartesian directions. The imaginary part of the dielectric function $\varepsilon_2(\omega)$ is related to $\sigma(\omega)$ by the equation $\varepsilon_2(\omega)=(4\pi/\omega)\sigma(\omega)$. The real part $\varepsilon_1(\omega)$ can be obtained from $\varepsilon_2(\omega)$ through the Kramers-Kronig relation, and the electron-energy-loss function is obtained from the complex dielectric function.

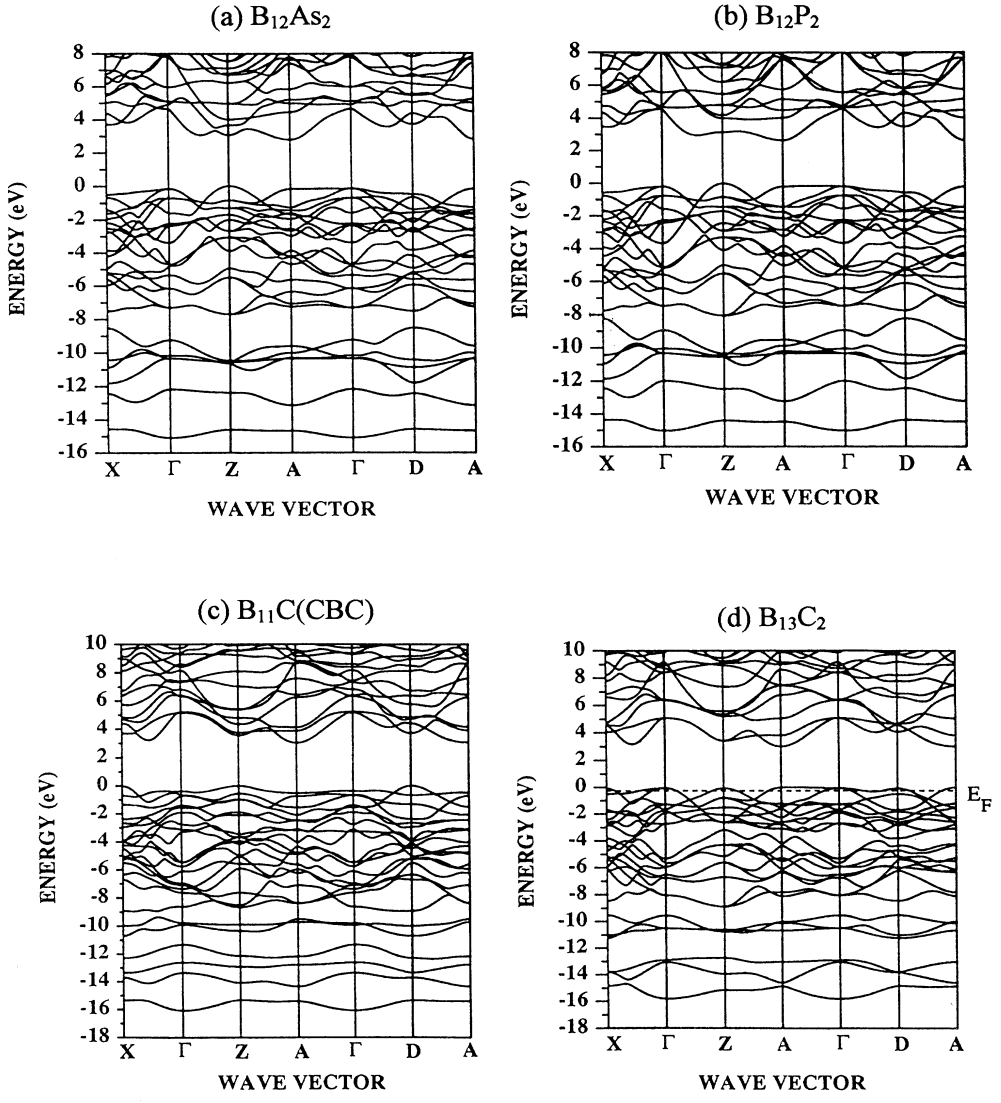

FIG. 2. Calculated band structures of (a) $B_{12}As_2$, (b) $B_{12}P_2$, (c) $B_{11}C(CBC)$, and (d) $B_{13}C_2$. The zero of energy is at the top of the VB, and the dotted line in (d) shows the Fermi level.

IV. ELECTRONIC STRUCTURES

Figure 2 shows the calculated energy bands of $B_{12}As_2$, $B_{12}P_2$, $B_{11}C(CBC)$, and $B_{13}C_2$ crystals along the symmetry axes of the BZ. $B_{12}As_2$, $B_{12}P_2$, and $B_1C(CBC)$ are found to be semiconductors having indirect band gaps. All have the top of the valence band (VB) at Z and the bottom of the conduction band (CB) at A. The gap values for $B_{12}As_2$, $B_{12}P_2$, and $B_{11}C(CBC)$ are 2.78, 2.63, and 3.03 eV, respectively. $B_{12}As_2$ and $B_{12}P_2$ have very similar band structures because of the similarity in the crystal structure, and the fact that As and P are isoelectronic. Our calculated gap values for $B_{12}As_2$ and $B_{11}C(CBC)$ are slightly larger than the values of 2.609 and 2.781 eV obtained from pseudopotential calculations.[24,26] In the case of $B_{12}As_2$, the calculated top of the VB at Z is 0.1 eV higher than the Γ point, which is the top of the VB in Ref. 24, but both calculations show that the energy values at the Γ and Z points are very close. There are some noticeable differences in the top of the VB region between $B_{11}C(CBC)$ and $B_{12}As_2$ or $B_{12}P_2$. For example, a single parabolic band of considerable curvature occurs at point D instead of point Z even though the energies at the two points are very close. Our calculation shows $B_{13}C_2$ to be a metal with the Fermi level 0.37 eV at the VB edge. We can consider this system to be an electron-deficient semiconductor with an intrinsic hole population at the top of the VB. Bylander and Kleinman[24] have also obtained a metallic band structure for $B_{13}C_2$ with an indirect band-gap value of 2.92 eV compared to our value 3.01 eV. Their Fermi energy is 0.372 eV below the top of the VB, the same as ours. In both calculations, the energy difference at X, Γ, D, and A are no more than 0.1 eV apart. The close agreement between the two calculations is a little surprising considering the different computational approaches used. Slack, Mcnelly, and Taft[13] measured the optical gaps of $B_{12}As_2$ and $B_{12}P_2$ to be 3.47 and 3.35 eV. They are larger than the calculated LDA gaps, but the relative order for the two crystals is correctly predicted. The direct and indirect gap values and the bandwidths for the four crystals are summarized in Table I.

Figure 3 shows the calculated total DOS's for $B_{12}As_2$, $B_{12}P_2$, $B_{11}C(CBC)$, and $B_{13}C_2$, respectively. For each crystal, there are four band segments within the VB region. We shall identify them as first, second, third, and fourth segments from top to bottom. The widths for the first segments are 7.69, 8.05, 8.95, and 8.85 eV, respectively, for the four crystals. For $B_{12}As_2$ and $B_{12}P_2$, each segment contains 34, 8, 2, and 2 electrons for a total of 46 valence electrons. For $B_{11}C(CBC)$, the number of electrons in each segment are 36, 4, 6, and 2 for a total of 48 valence electrons. In the case of $B_{13}C_2$, there are only 47

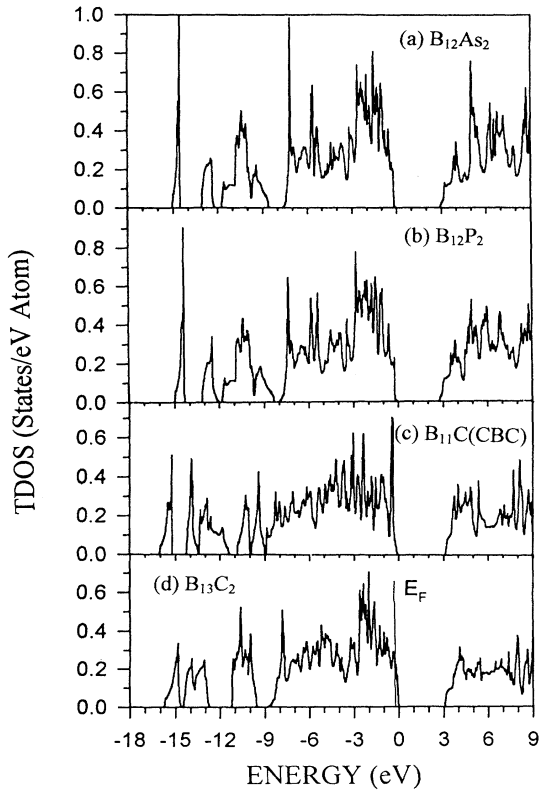

FIG. 3. Calculated total DOS. (a) $B_{12}As_2$. (b) $B_{12}P_2$. (c) $B_{11}C(CBC)$. (d) $B_{13}C_2$.

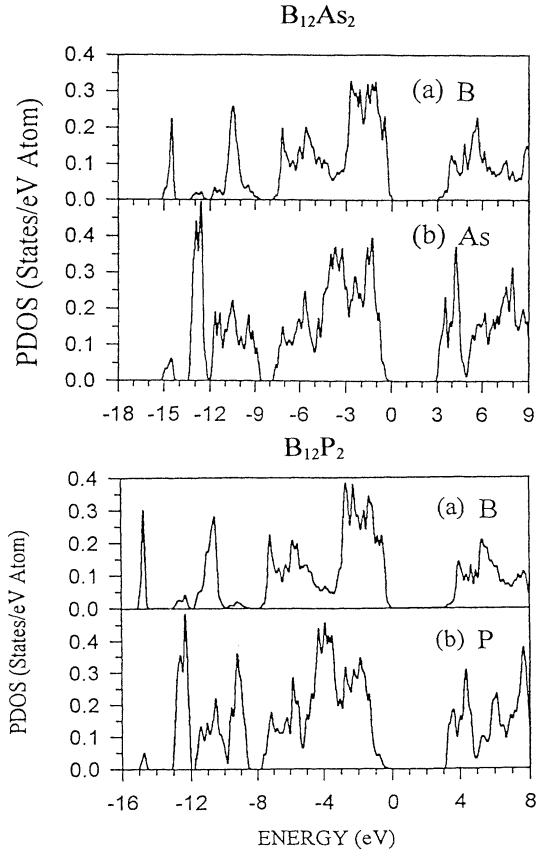

FIG. 4. PDOS of $B_{12}As_2$ and $B_{12}P_2$. (a) B. (b) As(P).

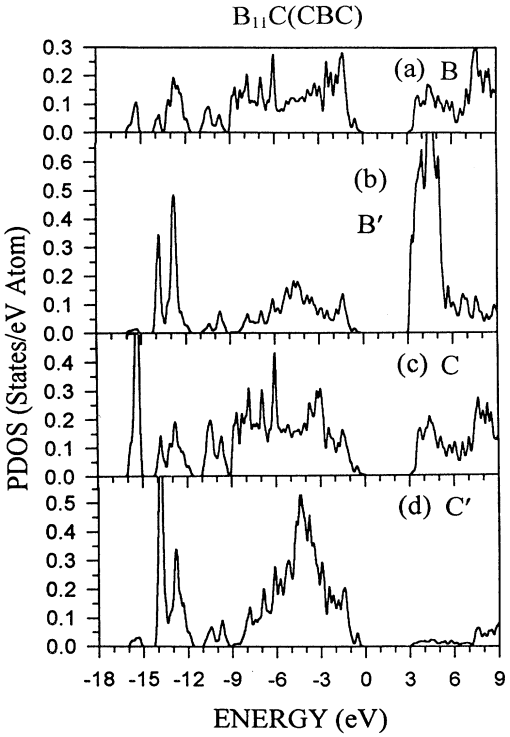

FIG. 5. PDOS of $B_{11}C(CBC)$. (a) B. (b) B′. (c) C. (d) C′.

valence electrons distributed over the four segments with 35, 6, 4, and 2 electrons in each segment. The odd number of valence electrons in the top segment results in an intrinsic hole at the top of the VB and a Fermi level only 0.37 eV below the VB top. More than 73% of valence electrons are distributed in the first segment. Among the four crystals, $B_{11}C(CBC)$ has the largest span of the total VB width of about 16.06 eV.

The atom-resolved PDOS per atoms for $B_{12}As_2$ and $B_{12}P_2$ are shown in Fig. 4, and that of $B_{11}C(CBC)$ and $B_{13}C_2$ in Figs. 5 and 6, respectively. To gain a better insight into the electronic bonding, the orbital-resolved PDOS's for $B_{12}As_2$ are presented in Fig. 7 for illustration. For both $B_{12}As_2$ and $B_{12}P_2$, valence electrons from B, As, or P atoms contribute uniformly to the first and second segments. However, distribution in the first segment comes mostly from the B $2p$ orbital electrons, and that in the second segments is from the s-orbital electrons. The density distribution in the second and third segments comes mostly from s-orbital electrons of As or P atoms. The fourth segments are dominated by B atoms, with s-orbital electrons having a higher distribution than that of p-orbital electrons. p-orbital and d-orbital electrons of As and P atoms also have significant distributions in the CB. Such orbital distributions of electrons in $B_{12}As_2$ and $B_{12}P_2$ indicate strong hybridization not just between the $2s$ and $2p$ electrons of B, but also between the s, p, and d

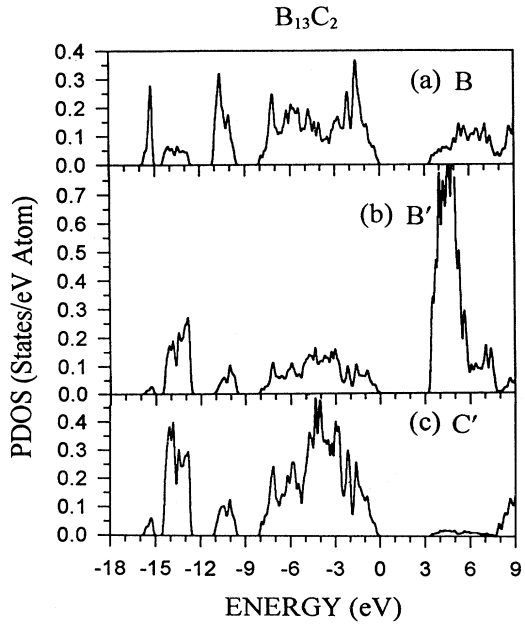

FIG. 6. PDOS of $B_{13}C_2$. (a) B. (b) B′. (c) C′.

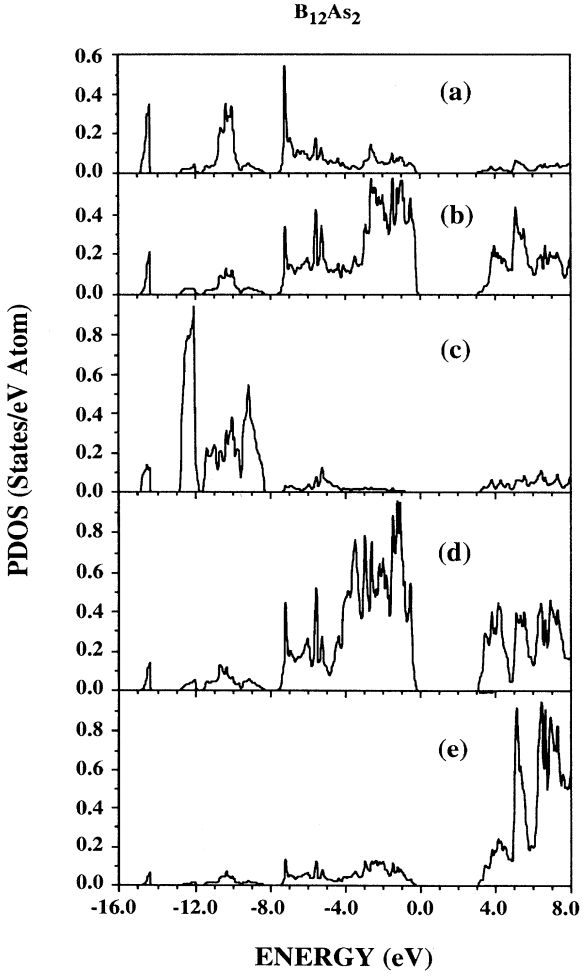

FIG. 7. Orbital-resolved PDOS of $B_{12}As_2$: (a) B-s, (b) B-p, (c) As-s, (d) As-p, and (e) As-d.

orbitals of As or P with that of B in a rather complicated bonding pattern.

For both $B_{11}C(CBC)$ and $B_{13}C_2$ crystals, PDOS's distributions of B and B′ atoms in Figs 5(a) and 5(b) or 6(a) and 6(b) are quite different, especially near the bottom of the CB. The DOS of the B′ atom is much higher than that of the other B atoms in the lower CB. This is because the B atom bonds to the other atoms in forming covalent bonds, while the B′ atom loses nearly one electron (see Sec. IV) to the two C′ atoms and is more likely in the $(B')^-$ valency state. Figures 5(c), 5(d), and 6(c) show the opposite situation for C and C′ atoms. In the CB region, the DOS distribution of the C′ atom is much lower than the C atom inside the icosahedron. Bullett[21] calculated the DOS for each atomic site of $B_{13}C_2$ and obtained similar results.

V. CRYSTAL BONDING

We have calculated valence-charge distributions for the four B_{12}-based crystals, and the results are presented as contour maps shown in Fig. 8. The contour plane has been chosen to contain the interstitial chain atoms. (As-As, P-P, or C′-B′-C′) and one B (B_2) atom bonded to the chain (shown in Fig. 1). These atoms are also properly labeled in Fig. 8. Figures 8(a) and 8(b) clearly show As-As or P-P covalent bonding, and the charges at the centers of both bonds are about 0.05. However, the charge value at the center of the As-B bond is only 0.08, and that for P-B bond is 0.07. For the $B_{11}C(CBC)$ crystal shown in Fig. 8(c), the extra C atom in the icosahedron modifies the charge distribution of the C′-B′-C′ chain slightly, while for $B_{13}C_2$ the distribution shows a more symmetric pattern along the C′-B′-C′ chain. The charge value at the center of the C-B bond along C′-B′-C′ chains are 0.15, almost triple the value at the center of the As-As or P-P bond. Thus the C′-B′-C′ bond is much more covalent than the As-As or P-P bond in the central chain. There are two low-density regions next to the interstitial chains for each crystal shown in Fig. 8. In the $B_{12}As_2$ case, it has a much lower charge value 0.01 in the middle part. For $B_{12}P_2$ the charge distribution is almost empty in the same area. That may be related to the large size of the As atom, causing a wide range distribution. Figures 8(c) and 8(d) show that $B_{13}C_2$ has more charge distribution in the middle of the low-density area than $B_{11}C(CBC)$.

The Mulliken effective charges for each type of atom in the four crystals have been calculated using a minimal basis set, and are listed in Table II. The main results can be summarized as follows: (1) the B_1 atoms at the top or bottom of the icosahedron gain almost no charge except in $B_{11}C(CBC)$ where a C atom substitutes for a B_1 atom in the icosahedron. (2) The equatorial B_2 atoms gain charge in $B_{12}As_2$ and $B_{12}P_2$, but lose charge in $B_{13}C_2$ and $B_{11}C(CBC)$. (3) The B′ atom in the chain loses 0.80 electron in $B_{13}C_2$ and 0.74 electron in $B_{11}C(CBC)$, respectively, to the neighboring C′ atoms in the chain. (4) The As-As (P-P) chain in the B_{12} As_2 ($B_{12}P_2$) loses 1.20 (0.90) electrons to the surrounding B icosahedra. On the other hand, the C′-B′-C′ chains in $B_{13}C_2$ and $B_{11}C(CBC)$ gain

TABLE II. Calculated Mulliken effective charge. The number in the parentheses indicates the number of atoms for the type.

Crystal	$B_{12}As_2$	$B_{12}P_2$	$B_{13}C_2$	$B_{11}C(CBC)$
B_1	3.01(6)	3.01(6)	3.02(4)	3.21(2)
			3.04(2)	3.14(2)
				2.98(1)
B_2	3.19(6)	3.14(6)	2.87(4)	2.75(2)
			2.92(2)	2.82(2)
				2.83(1)
				2.78(1)
As(P)	4.40(2)	4.55(2)		
C				4.28(1)
C′			4.66(2)	4.53(1)
				4.50(1)
B′			2.20(1)	2.26(1)

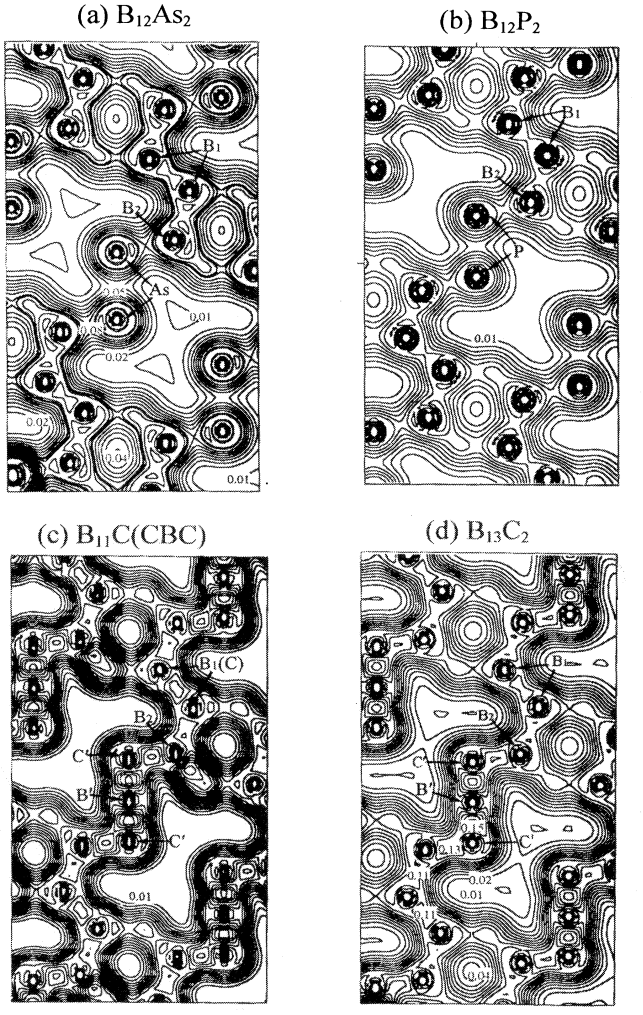

FIG. 8. Charge-density contour on a plane containing the interstitial chain and atoms in the icosahedron bonding to the chain. The contour lines are from 0.01 to 0.25 in the interval of 0.01 electron/(a.u.)^3. (a) $B_{12}As_2$. (b) $B_{12}P_2$. (c) $B_{11}C(CBC)$. (d) $B_{13}C_2$.

0.52 and 0.29 electrons, respectively. This indicates that $B_{12}As_2$ and $B_{12}P_2$ are more ionic than $B_{13}C_2$ and $B_{11}C$(CBC) crystals. The stronger covalent bonds in the intericosahedral chains explain the nature of the inverse molecular solids mentioned earlier.[10] Thus we expect $B_{11}C$(CBC) to be the hardest material among the four crystals. We also see that by substituting one B_1 atom in the icosahedron by a C atom which tends to draw charge, the charge transfer from the central C'-B'-C' chain is minimized, resulting in a stronger intericosahedral covalent bonding. The above scenario is consistent with the notion that any electron deficiency in the intraicosahedral bonding relative to the intericosahedral bonding tends to make the icosahedra more compressible than the structural medium surrounding the icosahedra. It is also interesting to point out that the uneven charge distribution on the three-atom chain in $B_{13}C_2$ and $B_{11}C$(CBC) will have some bearing on the hopping conductivity and small-polaron formation in these crystals.[2,18]

Table III lists the calculated overlap population or bond order in the four crystals. Results for the α-r-B_{12} crystal are also included for comparison. We classify the bonding to be of three types: (A) intraicosahedral bonding, (B) intericosahedral bonding, and (C) intrachain bonding. As can be seen, the intericosahedral B_1-B_1 bonding is very strong, almost twice that of the intraicosahedral bonding. Also, the intrachain bonding in $B_{13}C_2$ and $B_{11}C$(CBC) is much stronger than intrachain As-As or P-P bonding in $B_{12}As_2$ or $B_{12}P_2$. The weakest bonding is the intericosahedral B_2-B_2 bonding in α-r-B_{12}, which is the weak bonding between equatorial B atoms of different icosahedra. The results of Table III are fully consistent with the effective charge calculations and the analysis of the previous paragraph on interatomic bonding.

TABLE III. Calculated overlap populations for B_{12}-related crystals. (A) Intraicosahedral bonding. (B) Intericosahedral bonding. (C) Intrachain bonding.

Crystal	type	$B_{12}As_2$	$B_{12}P_2$	$B_{13}C_2$	$B_{11}C$(CBC)	α-rB_{12}
B_1-B_1	(A)	0.12(6)	0.11(6)	0.13(6)	0.13(4)	0.12(6)
B_1-B_2	(A)	0.13(12)	0.11(12)	0.13(12)	0.13(10)	0.12(18)
	(A)	0.10(6)	0.09(6)	0.11(6)	0.12(5)	
B_2-B_2	(A)	0.13(6)	0.11(6)	0.14(6)	0.11(6)	0.14(6)
B_1-C	(A)				0.11(2)	
B_2-C	(A)				0.12(2)	
	(A)				0.11(1)	
B_1-B_1	(B)	0.25(6)	0.27(6)	0.24(6)	0.24(4)	0.24(6)
B_2-B_2	(B)					0.05(12)
B_2-As(P)	(B)	0.21(6)	0.27(6)			
B_1-C	(B)				0.22(2)	
B_2-C'	(B)			0.20(6)	0.21(6)	
As-As,P-P	(C)	0.15(1)	0.15(1)			
B'-C'	(C)			0.28(2)	0.27(2)	

VI. TOTAL ENERGY

The total energies for the four crystals are calculated as functions of the crystal volume. The results are shown in Fig. 9, where V_0 is the equilibrium cell volume listed in Table I. Calculations were performed for at least eight points close to the equilibrium values of V/V_0 by uniformly scaling the lattice constant. In each calculation, the electron-fitting error is kept to less than 0.01 electron per valence electron to ensure the desired level of precision. Our calculations give the equilibrium lattice constants to be within 1% of the measured values for $B_{12}As_2$, $B_{12}P_2$, and $B_{13}C_2$, and within 1.5% for $B_{11}C$(CBC). This level of accuracy is similar to our recent calculations in other crystals using the same method.[35–38] We obtained the bulk moduli for these crystals by fitting the E vs V/V_0 curves to Munaghan's equation of state.[34] Our results are listed in Table IV, which also contains the result for α-r-B_{12} from the earlier study.[12] Results of several existing calculations are also listed for comparison.[16,23,25] In general, our calculated bulk moduli are larger than that of Lee, Bylander, and Kleinman[25] using the first-principles pseudopotential method. The same is also true for α-r-B_{12}. However, the relative order for $B_{12}As_2$, $B_{13}C_2$, and $B_{11}C$(CBC) is the same in both calculations.

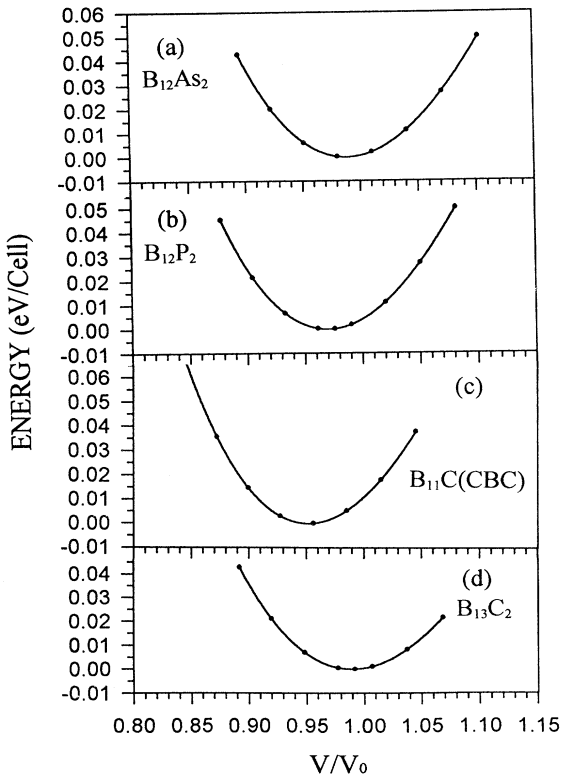

FIG. 9. Calculated total energies vs (V/V_0). (a) $B_{12}As_2$. (b) $B_{12}P_2$. (c) $B_{11}C$(CBC). (d) $B_{13}C_2$.

TABLE IV. Calculated total-energy results for B_{12}-related crystals.

	$B_{12}As_2$	$B_{12}P_2$	$B_{13}C_2$	$B_{11}C(CBC)$	α-$r$$B_{12}$
V_{min}/V_0	0.990	0.976	0.987	0.955	0.994[a]
B (Mbar)	2.50	2.66	2.63	2.73	2.45[a]
	1.817[b]		2.169[b]	2.339[b]	2.02[b]
					2.49[c] 2.66[c]
				2.47[d]	
Expt.					

[a]Reference 10.
[b]Reference 25.
[c]Reference 23.
[d]Reference 16.

In the $B_{11}C(CBC)$ crystal, Gieske, Aselage, and Emin have deduced the elastic moduli value from ultrasonic velocity measurement.[16] Their value of 2.47 Mbar is between our calculated value of 2.73 Mbar and the value of 2.34 Mbar from Ref. 26. It is conceivable that our calculated bulk modulus values for the four crystals are upper limits only, since we did not optimize all the structure parameters in the total-energy calculation. Among the five crystals studied, $B_{11}C(CBC)$ has the highest bulk modulus which is consistent with the strong intrachain bonding in this crystal discussed in Sec. III. Since α-r-B_{12} has the smallest calculated bulk modulus, it can be concluded that the interstitial chains increase the hardness of the B_{12}-based materials because of the stronger intrachain covalent bonding.

VII. OPTICAL TRANSITIONS

The interband optical conductivities σ of $B_{12}As_2$, $B_{12}P_2$, $B_{11}C(CBC)$, and $B_{13}C_2$ crystals were calculated from the *ab initio* wave functions. They were converted into complex dielectric functions and energy-loss functions. The results are presented in Fig. 10.

$B_{12}As_2$ has an absorption threshold of 3.09 eV arising from the direct band-gap transition at Z. The $\sigma(\omega)$ shows the structures at 6.73, 8.71, 10.82, and 15.78 eV with sharp minima at 9.52 and 13.08 eV. The conductivity curve for $B_{12}P_2$ is quite different from that of $B_{12}As_2$, although the threshold energy of 3.11 eV is very close. It has a major peak at 6.37 eV, and a very broad peak near

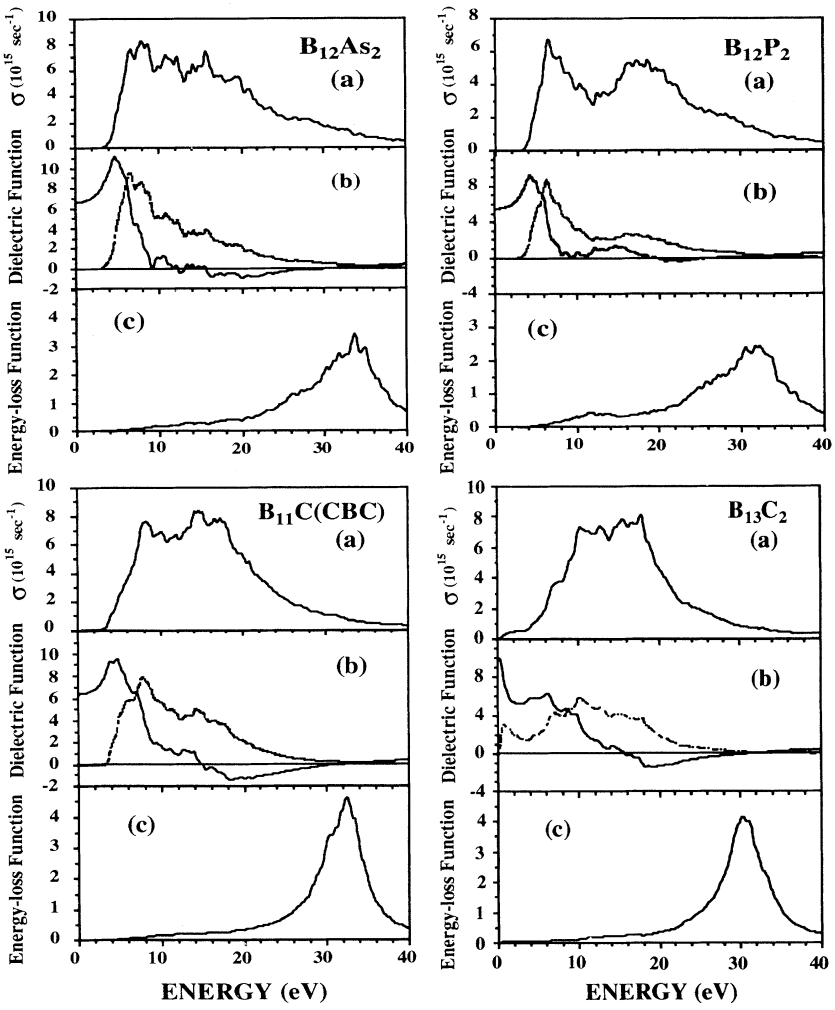

FIG. 10. Calculated optical properties of $B_{12}As_2$, $B_{12}P_2$, $B_{11}C(CBC)$, and $B_{13}C_2$: (a) σ, (b) ε_1 (solid line) and ε_2 (dashed line), and (c) energy-loss function.

TABLE V. Calculated static dielectric constants ε_0, the major peak position of $\varepsilon_2(\omega)$, and the bulk-plasmon frequency ω_p.

	$B_{12}As_2$	$B_{12}P_2$	$B_{13}C_2$	$B_{11}C$(CBC)	α-r-B_{12}
ε_0	6.59	5.49		6.35	7.31
Major peak position (eV)	6.73	6.37	9.97	7.72	6.90
ω_p (eV)	33.7	31.7	30.2	32.7	30.3

18 eV with a minimum at 11.9 eV. Thus the optical conductivities of $B_{12}As_2$ and $B_{12}P_2$ are sufficiently different even though their ground-state electronic structures are very similar. The energy-loss functions show plasmon peaks ω_p for the two crystals to be at 33.7 and 31.7 eV, respectively. The static dielectric constant ε_0 estimated from the zero-frequency limits of the real part of the dielectric functions are 6.59 and 5.49 for $B_{12}As_2$ and $B_{12}P_2$, respectively.

The optical conductivity curve for $B_{11}C$(CBC) is quite different from that of $B_{12}As_2$ or $B_{12}P_2$. The rate of increase in absorption above the threshold of 3.20 eV and up to 7 eV is less steep, and there is a plateaulike region between 8 and 18 eV. Peak structures at 7.9, 10.3, and 17.4 eV can be identified. The static dielectric constant and the plasma frequency are estimated to be 6.35 and 32.7 eV respectively. Samara *et al.*[18] had measured the dielectric functions of several B_xC compounds with $x=4.33$, 4.5, 5.5, and 9.0 corresponding to the C composition range of 9–19 %. They obtained the electronic contribution to the real part of the dielectric function $\varepsilon_1(\omega)$ in the high-frequency limit. For B_4C and B_9C, estimated values of $\varepsilon_1(0)$ of 6.7 ± 0.3 and 7.0 ± 0.3 were obtained, which are slightly larger than the earlier result of close to 6.0 obtained by the same group on smaller specimens. These numbers are certainly consistent with our calculated value of 6.35 for $B_{11}C$(CBC).

The optical conductivity of $B_{13}C_2$ is rather different from the other three B_{12}-based semiconductor crystals. Because $B_{13}C_2$ is electron deficient with an intrinsic hole at the top of the VB, there can be intraband transition for electrons below the Fermi level to the intrinsic hole above. This leads to a sharply increased $\varepsilon_1(\omega)$ as $\omega\rightarrow0$. This result is in line with the experimental finding of Samara *et al.*[18] that the electronic dielectric constant of B_9C is larger than that of B_4C. Transitions below 3 eV in $B_{13}C_2$ are clearly of intraband type, and those above 3 eV are interband transitions which resemble that of $B_{11}C$(CBC) except for a shoulderlike structure at 7 eV and the plateaulike region between 10 and 18 eV. The plasmon peak in $B_{13}C_2$ is at 30.3 eV, almost 2.5 eV below that of $B_{11}C$(CBC). The calculated values of ε_0, ω_p, and the first major peak positions in the $\varepsilon_2(\omega)$ spectra for the four crystals together with that of α-r-B_{12} (Ref. 12) are summarized in Table V.

VIII. CONCLUSIONS

We have studied the electronic structure and bonding in four B_{12}-based compounds by means of a first-principles method. We show that $B_{12}As_2$, $B_{12}P_2$, and $B_{11}C$(CBC) are semiconductors, while $B_{13}C_2$ is a metal with one electron deficient in an otherwise semiconductorlike band structure. These results are in close agreement with other existing first-principles calculations using the pseudopotential-plane-wave method. The interatomic bonding in these crystals is studied by calculating the effective charges and overlap populations in these crystals. It is concluded that intericosahedral bonding is stronger than intraicosahedral bonding, providing an explanation for the inverse molecular solids. Of particular significance is the strong covalent bonding in the intericosahedral chain in $B_{11}C$(CBC) which explains the superior mechanical properties of the refractory ceramic compound B_4C. Equilibrium lattice constants and bulk moduli in these crystals are also studied by total-energy calculations. Our calculated bulk moduli are to be considered as upper limits because of our inability to relax the internal coordinates under pressure. The optical properties of these four crystals show a very similar pattern except for $B_{13}C_2$ at the low-frequency limit which shows metallic conductivity. Our calculated electronic portion of the static dielectric constants for the semiconducting crystals are in good agreement with recent experimental measurements. We intend to use a similar approach to study the electronic and optical properties of other B-rich compounds in order to obtain a full understanding of this class of fascinating materials with the same very outstanding properties.

ACKNOWLEDGMENT

This work was supported by the U.S. Department of Energy under Grant No. DE-FG02-84DR45170.

[1] *The Chemistry of Boron and Its Compounds,* edited by E. L. Muetterties (Wiley, New York, 1967).

[2] D. Emin, Phys. Today **40** (1), 55 (1987).

[3] *Boron Rich Solids,* edited by D. Emin, T. L. Aselage, C. L. Beckel, I. A. Howard and C. Wood, AIP Conf. Proc. No. 140 (AIP, New York, 1986).

[4] *Boron Rich Solids,* edited by D. Emin, T. L. Aselage, A. C. Switendick, B. Morosin, and C. L. Beckel, AIP Conf. Proc. No. 231 (AIP, New York, 1991).

[5] *Boron, Borides and Related Compuonds,* Proceedings of the 11th International Symposium on Boron, Borides and Related Compounds, Tsukuba, Japan, 1994, edited by R. Uno and I. Higashi [Jpn. J. Appl. Phys. Series 10 (1994)].

[6] J. L. Hoard and R. E. Hughes, in *The Chemistry of Boron and Its Compounds* (Ref. 1), p. 25; H. L. Yakes, in *Boron Rich Solids* (Ref. 3), p. 97.

[7]*Boron and Refractory Borides,* edited by V. I. Matkovich (Springer-Verlag, Berlin, 1977).
[8]H. C. Longuet-Higgins and M. de V. Roberts, Proc. R. Soc. London Ser. A **230**, 110 (1955); W. N. Lipscomb, J. Less-Common Metals **82**, 1 (1981).
[9]D. W. Bullett, J. Phys. C **15**, 415 (1982); also A. C. Larson, in *Boron Rich Solids* (Ref. 3), p. 109.
[10]R. J. Nelmes, J. S. Loveday, R. M. Wilson, W. G. Marshall, J. M. Besson, S. Klotz, G. Hamel, T. L. Aselage, and S. Hull, Phys. Rev. Lett. **74**, 2268 (1995).
[11]W. Y. Ching, M.-Z. Huang, Y.-N. Xu, W. G. Harter, and F. T. Chan, Phys. Rev. Lett. **67**, 2045 (1991).
[12]D. Li, Y.-N. Xu, and W. Y. Ching, Phys. Rev. B **45**, 5895 (1992).
[13]G. A. Slack, T. F. Mcnelly, and E. A. Taft, J. Chem. Phys. Solids **44**, 1009 (1983).
[14]T. L. Aselage and D. Emin, in *Boron Rich Solids* (Ref. 4), p. 177.
[15]B. Morosin, T. L. Aslage, and D. Emin, in *Boron Rich Solids* (Ref. 4), p. 193.
[16]J. H. Gieske, T. L. Aselage, and D. Emin, in *Boron Rich Solids* (Ref. 4), p. 376.
[17]J. Kawai, K. Maeda, I. Higashi, M. Takami, Y. Hayasi, and M. Uda, Phys. Rev. B **42**, 5693 (1990).
[18]G. A. Samara, H. L. Tardy, E. L. Venturini, T. L. Aselage, and D. Emin, Phys. Rev. B **48**, 1468 (1993).
[19]T. L. Aselage, D. Emin, G. A. Samara, D. R. Tallant, S. B. Van Deusen, M. O. Eatongh, H. L. Tardy, E. L. Venturini, and S. M. Johnson, Phys. Rev. B **48**, 11 759 (1993).
[20]M. Takeda, K. Kimura, A. Hori, H. Yamashita, and H. Ino, Phys. Rev. B **48**, 13 159 (1993).
[21]D. W. Bullett, in *Boron Rich Solids* (Ref. 3), p. 249.
[22]M. M. Florence and C. L. Beckel, in *Boron Rich Solids* (Ref. 4), p. 37.
[23]C. Mailhiot, J. B. Grant, and A. K. McMahan, Phys. Rev. B **42**, 9033 (1990).
[24]D. M. Bylander, L. Kleinman, and S. Lee, Phys. Rev. B **42**, 1394 (1990); D. M. Bylander and L. Kleinman, *ibid.* **43**, 1487 (1990).
[25]S. Lee, D. M. Bylander, and L. Kleinman, Phys. Rev. B **45**, 3245 (1992).
[26]I. Morrison, D. M. Bylander, and L. Kleinman, Phys. Rev. B **45**, 1533 (1992).
[27]I. Morrison, D. M. Bylander, and L. Kleinman, Phys. Rev. B **45**, 10 872 (1992); S. Lee, D. M. Bylander, S. W. Kim, L. Kleinman, *ibid.* **45**, 3248 (1992).
[28]M. Takeda, A. Hori, H. Yamashita, and K. Kimura, Mater. Trans. JIM **34**, 128 (1993).
[29]B. Morosin, A. W. Mullendore, D. Emin, and G. A. Slack, in *Boron Rich Solids* (Ref. 3), p. 70.
[30]W. Y. Ching, J. Am. Ceram. Soc. **73**, 3135 (1990).
[31]E. Wigner, Phys. Rev. **46**, 1002 (1934).
[32]R. S. Mulliken, J. Am. Chem. Soc. **77**, 887 (1954).
[33]I. Tanaka and K. Niihara, J. Am. Ceram, Soc. **76** (11), 2833 (1993).
[34]F. D. Murnaghan, Proc. Natl. Acad. Sci. U.S.A. **30**, 244 (1944).
[35]Y.-N. Xu and W. Y. Ching, Phys. Rev. B **48**, 4335 (1993).
[36]W. Y. Ching and Y.-N. Xu, J. Am. Ceram. Soc. **77** (2), 404 (1994).
[37]H. Yao and W. Y. Ching, Phys. Rev. B **50**, 11 231 (1994).
[38]S. Mo and W. Y. Ching, Phys. Rev. B **51**, 13 023 (1995).